A Biphase Modulator Circuit for Impulse Radio-UWB Applications

Bernd Schleicher, *Student Member, IEEE*, Çagri A. Ulusoy, and Hermann Schumacher, *Member, IEEE*

***Abstract*—This letter presents a circuit to provide binary phase shift keying to ultra-wideband (UWB) impulse transmitters. The circuit is based on a Gilbert-cell multiplier and uses active on-chip balun and unbalanced-to-balanced converters for single-ended to single-ended operation. Detailed measurements of the circuit show a gain ripple of ± 1 dB at an overall gain of -2 dB, an input reflection below -12 dB, an output reflection below -18 dB, a group delay variation below 6 ps and a -1 dB input compression point of more than 1 dBm in both switching states over the full 3.1–10.6 GHz UWB frequency range. A time domain measurement verifies the switching operation using an FCC-compliant impulse generator. The circuit is fabricated in a $0.8\ \mu$m Si/SiGe HBT technology, consumes 31.4 mA at a 3.2 V supply and has a size of $510 \times 490\ \mu\text{m}^2$, including pads. It can be used in UWB systems using pulse correlation reception or spectral spreading.**

***Index Terms*—Biphase modulator, impulse radio ultra-wideband (IR-UWB).**

I. Introduction

SEVERAL methods to generate ultra-wideband (UWB) impulses have been reported in the literature (e.g., [1]–[3]). Most of them are targeting the FCC UWB spectral mask. The modulation techniques that can be realised with these impulse generators are typically on-off-keying (OOK) or pulse position modulation (PPM). In both cases, the impulse orientation remains unchanged. When using a coherent demodulation, biphase modulation is more advantageous in terms of bit error rate (BER) performance for AWGN channels than conventional OOK and PPM, since it increases the Euclidian distance between the symbols. This has been pointed out for UWB systems by Güvenç and Arslan [4]. Biphase modulation needs the ability to switch between an impulse and its inverted replica, a capability usually missing in UWB transmitters. One of the few implementations so far was published by Terada and co-workers [5], who used differential pulse generation and a cross-coupling MOS switch matrix. In contrast, the solution presented here is single-ended and compatible with many existing pulse generators.

Manuscript received June 10, 2009; revised October 30, 2009. First published January 19, 2010; current version published February 10, 2010. This work was supported by the SiGe foundry of Telefunken Semiconductors, Heilbronn, Germany. This project is funded by the German research foundation (DFG) by means of the priority programme UKoLoS.

The authors are with the Institute of Electron Devices and Circuits and the Competence Center on Integrated Circuits in Communications, Ulm University, Ulm, Germany (e-mail: bernd.schleicher@uni-ulm.de; ahmet.ulusoy@uni-ulm.de; hermann.schumacher@uni-ulm.de).

Color versions of one or more of the figures in this letter are available online at http://ieeexplore.ieee.org.

Digital Object Identifier 10.1109/LMWC.2009.2038617

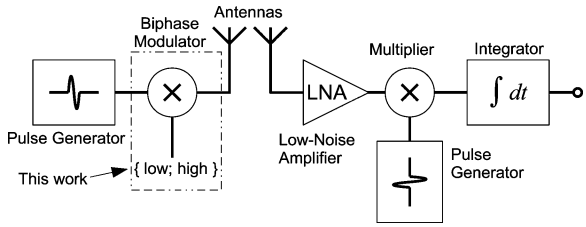

Fig. 1. Sample system schematic of a typical correlation type UWB transceiver system.

Fig. 1 shows a sample transceiver schematic for a correlation type system. The biphase modulator is placed between the transmit pulse generator and the antenna. Apart from the use of the biphase modulator in a correlation system, the circuit can as well be used in a spread-spectrum system for the chipwise spreading and despreading of multi-impulse symbols, as proposed in [6]. The modulator circuit presented in this letter can be used for both types of applications.

II. Circuit Concept

The fundamental operation of the modulator circuit is similar to the multiplication of the high-frequency impulse with a positive or negative switching signal. A multiplication of the impulse with a positive switching signal results in a non-inverted output impulse and the multiplication with a negative switching signal inverts the impulse. A simplified circuit schematic of the biphase modulator can be seen in Fig. 2. At its core, a four-quadrant multiplier based on a double balanced Gilbert cell topology is chosen. The upper four transistors (transistor quad) of the Gilbert cell (T_1, T_2, T_3 and T_4) are optimized as signal switches. The switching signal activates either transistors T_1, T_4 or T_2, T_3. If in one switching state e. g. T_1 is off, the current flowing through R_1 passes through T_3. This ensures that the current flow is not interupted and the voltage level does not rise up to the supply voltage level, distorting the correct operation. Therefore a double balanced topology is necessary and can not be reduced to only half of the circuit. When operated in one of the switching states the Gilbert cell core circuit is regarded as a differential cascode stage. The lower two transistors (transistor pair) of the Gilbert-cell (T_5 and T_6) are optimized for high linearity and wide bandwidth by applying feedback with the resistances R_3 and R_4 and the peaking capacitance C_1. An approximately unit gain between input and output is targeted.

Since the Gilbert-cell is a fully differential circuit, all input signals need to be converted from single-ended to differential and the output signal needs to be converted back. This is done for the switching input by a threshold switch circuit. By changing

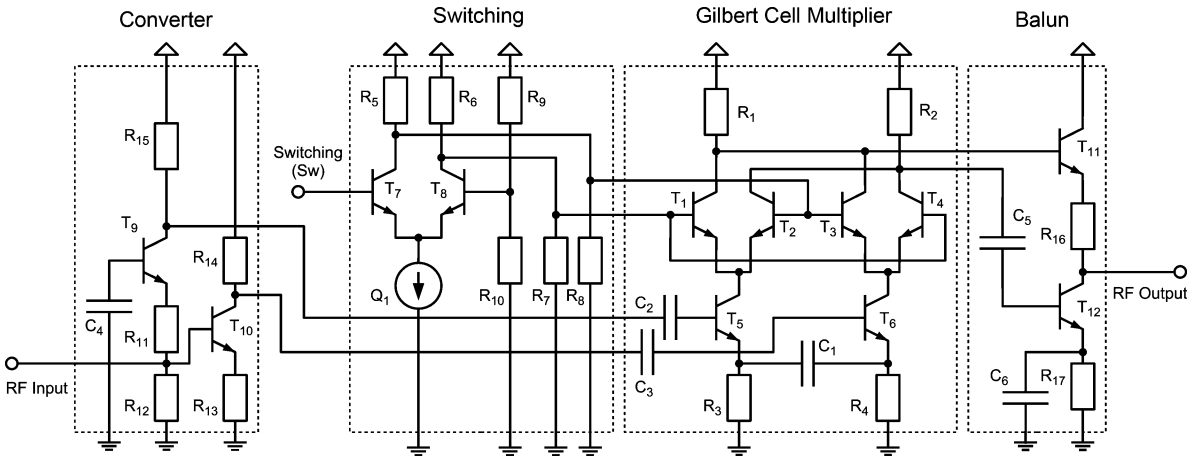

Fig. 2. Simplified circuit schematic of the biphase modulator. Only part of the bias arrangement is shown here.

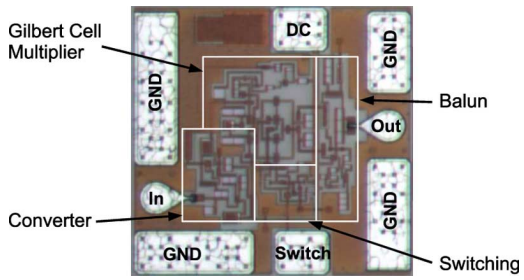

Fig. 3. Micrograph of the fabricated biphase modulator circuit, indicating the circuit's ports and building blocks.

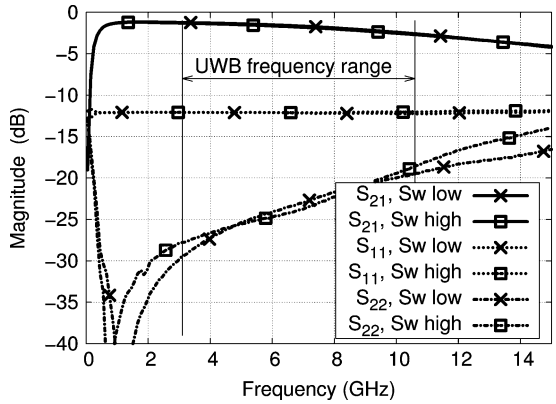

Fig. 4. Measured S-parameter magnitudes in both switching states.

the voltage level of the input voltage divider, formed by resistances $\mathrm{R_5}$, $\mathrm{R_8}$ and transistor $\mathrm{T_7}$ on one side and $\mathrm{R_6}$, $\mathrm{R_7}$ and $\mathrm{T_8}$ on the other side, a change of the current flow through the transistors is forced and the differential switching voltage for the Gilbert-cell is generated. The input switching signal (Sw) was adjusted to be 0 V for the low and 2 V for the high switching state.

The single-ended impulse signals at the RF input of the modulator circuit are converted to differential signals by an unbalanced-to-balanced converter. The converter topology used in this circuit uses the non-inverting behavior of transistor $\mathrm{T_9}$ in common-base configuration and the inverting behavior of $\mathrm{T_{10}}$ in common-emitter configuration. A big advantage of this topology is that the input matching can be easily adjusted by $\mathrm{R_{11}}$ and $\mathrm{R_{12}}$. The differential output signal is converted to single-ended using the balanced-to-unbalanced converter (balun) with transistors $\mathrm{T_{11}}$ and $\mathrm{T_{12}}$ in a push-pull configuration. $\mathrm{R_{17}}$ and $\mathrm{C_6}$ improve linearity and gain balance between the two inputs. The output impedance can be adjusted by $\mathrm{R_{16}}$. The IC was fabricated in a commercially available $0.8\ \mu\mathrm{m}$ Si/SiGe HBT technology [7]. A micrograph of the circuit can be seen in Fig. 3. The IC has an overall size of $510 \times 490\ \mu\mathrm{m}^2$.

III. Measurement Results

The IC is characterized on-wafer by several measurements. The measured S-parameters magnitudes are shown in Fig. 4. The curves are very similar for low and high switching states. The measured gain $(\mathrm{S_{21}})$ is around $-2\ \mathrm{dB}$ within a variation of $\pm 1\ \mathrm{dB}$. The measured input $(\mathrm{S_{11}})$ and output $(\mathrm{S_{22}})$ matching coefficients remain below $-12\ \mathrm{dB}$ and $-18\ \mathrm{dB}$, respectively for the complete UWB frequency range. The measured reverse isolation $(\mathrm{S_{12}})$ is below $-40\ \mathrm{dB}$ between 3.1–10.6 GHz. Fig. 5 shows the measured phase of the transmission coefficient $(\mathrm{Phase_{21}})$. The change in phase of 180° between the two switching states is maintained over the full UWB bandwidth. The extracted group delay of the circuit is also shown in Fig. 5. The small group delay variation, below 6 ps in the complete UWB frequency range, together with the small gain variation indicate only minor distortions to the incoming UWB impulse.

To prove this in time domain, a UWB impulse was applied to the input of the modulator and the output waveform was measured with an equivalent-time sampling oscilloscope. The used impulse is generated by the FCC-compliant impulse generator presented in [8]. Fig. 6 shows the time domain output of the modulator in the two switching states and for comparison the impulse, when connecting a through line from the calibration substrate instead of the modulator to the measurement setup. It can be seen that the biphase switching clearly takes place and that both impulses are only a scaled version of the through connected impulse, but the impulse shapes remain unchanged.

In Fig. 7 the measurement of a modulated impulse sequence at an elevated repetition rate of 200 MHz, together with the return-to-zero (RZ) coded impulse trigger signal and the modu-

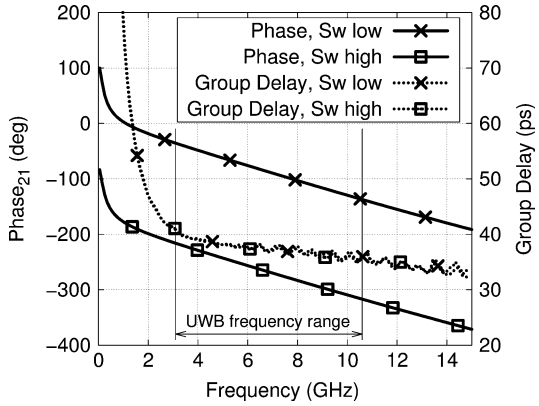

Fig. 5. Measured phase in both switching states, showing the modulator's wideband phase inversion. Group delay was extracted from the phase of S_{21} and is constant within ± 3 ps.

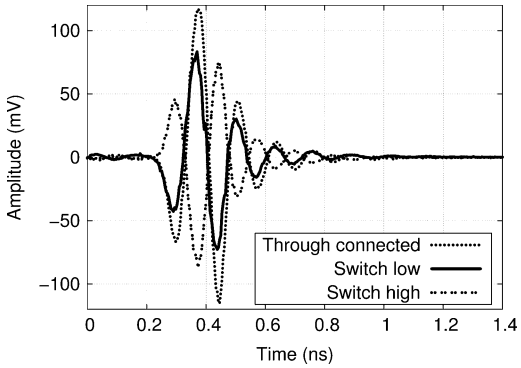

Fig. 6. Measured time domain output of the modulator in both switching states when fed by an FCC-compliant impulse at the input. For comparison the signal when connecting a through instead of the modulator is shown.

lating data signal is shown. The distortions due to switching remain below -25 dB and will further decrease, when using a switching signal with a lower slew rate. To determine the linearity performance of the biphase modulator a sinusoidal stimulus was applied to the circuit at different frequencies and varied in input power. Losses of the cables and probes were carefully determined and compensated during the measurement. Fig. 8 plots the -1 dB input compression point versus frequency. The input compression point stays above 1 dBm over the complete UWB frequency range and for both switching states. The circuit has a DC consumption of 31.4 mA at a 3.2 V bias in both switching states.

IV. Conclusion

This letter presented the successful implementation of a biphase modulator circuit for IR-UWB systems with single-ended inputs and output. The measured performance showed a distortionless operation of the circuit in the FCC-allocated UWB frequency range. Therefore an integration of the circuit into a UWB system can be easily realized.

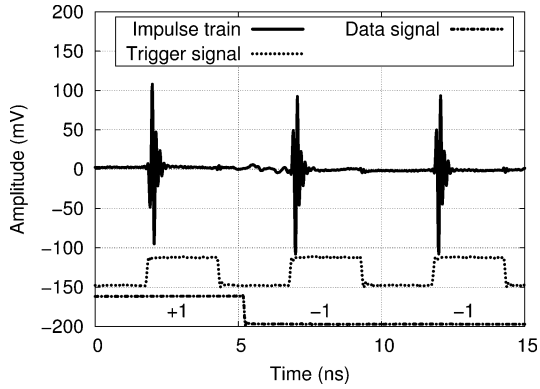

Fig. 7. Measured modulated 200 MHz impulse sequence, including the RZ coded impulse trigger signal and the modulation data signal.

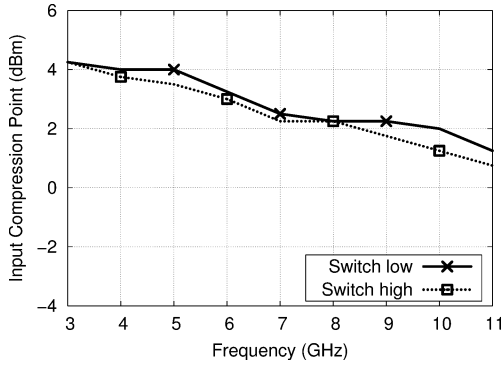

Fig. 8. Measured -1 dB input compression point versus frequency.

References

[1] A. Cacciatori, L. Lorenzi, and L. Colalongo, "A power efficient HBT pulse generator for UWB radars," in *Proc. IEEE Int. Symp. Circuits Syst. (ISCAS)*, New Orleans, LA, May 2007, pp. 3916–3919.

[2] T. Norimatsu, R. Fujiwara, M. Kokubo, M. Miyazaki, A. Maeki, Y. Ogata, S. Kobayashi, N. Koshizuka, and K. Sakamura, "A UWB-IR transmitter with digitally controlled pulse generator," *IEEE J. Solid-State Circuits*, vol. 42, no. 6, pp. 1300–1309, Jun. 2007.

[3] J. Dederer, A. Trasser, and H. Schumacher, "A SiGe monocycle impulse generator for impulse radio ultra-wideband applications," in *Proc. German Microw. Conf. (GeMIC)*, Karlsruhe, Germany, 2006, [CD ROM].

[4] I. Güvençç and H. Arslan, "On the modulation options for UWB systems," in *Proc. IEEE Military Commun. Conf. (MILCOM)*, Oct. 2003, vol. 2, pp. 892–897.

[5] T. Terada, S. Yoshizumi, Y. Sanada, and T. Kuroda, "Transceiver circuits for pulse-based ultra-wideband," in *Proc. Int. Symp. Circuits Syst. (ISCAS)*, Vancouver, BC, Canada, May 2004, vol. 4, pp. 349–352.

[6] T. Thiasiriphet and J. Lindner, "A novel comb filter based receiver with energy detection for UWB wireless body area networks," in *Proc. IEEE Int. Symp. Wireless Commun. Syst. (ISWCS)*, Reykjavik, Iceland, Oct. 2008, pp. 498–502.

[7] A. Schüppen, J. Berntgen, P. Maier, M. Tortschanoff, W. Kraus, and M. Averweg, "An 80 GHz SiGe production technology," *III-Vs Rev.*, vol. 14, no. 6, pp. 42–46, Aug. 2001.

[8] J. Dederer, B. Schleicher, F. de Andrade Tabarani Santos, A. Trasser, and H. Schumacher, "FCC compliant 3.1–10.6 GHz UWB pulse radar system using correlation detection," in *IEEE MTT-S Int. Dig.*, Honolulu, HI, Jun. 2007, pp. 1471–1474.